JOURNAL OF MATERIALS SCIENCE 28 (1993) 823–829

Microstructure of Ni–10Co–8Cr–4W–13Zr alloy and its bonding behaviour for single-crystal nickel-base superalloy

Y. ZHENG, L. ZHAO, K. TANGRI
Metallurgical Science Laboratory, Department of Mechanical and Industrial Engineering, University of Manitoba, Winnipeg, Manitoba, Canada, R3T 2N2

In the later stages of solidification of zirconium-containing superalloys, the concentration of zirconium in the interdendritic melts is above 10 wt %. The γ dendrites formed in the early stage of solidification may be considered to be joined by the interdendritic zirconium-rich melt. Based on the composition of the zirconium-rich melt, an Ni–10Co–8Cr–4W–13Zr (wt %) alloy was selected as an interlayer alloy for brazing and transient liquid-phase (TLP) bonding of single crystal superalloys. All the elements in the interlayer alloy are beneficial to the single-crystal superalloys. A bonding microstructure which is very similar to that of the base alloy was obtained by means of the TLP process using this interlayer alloy. In the present work, the microstructural characteristics of the interlayer alloy and the phase relationships in the bond during brazing and TLP processes were investigated.

1. Introduction

Single-crystal nickel-base superalloys have been widely used in the manufacture of aeroengine blades. Unfortunately, it is very difficult to fusion-weld this kind of alloy due to the high content of aluminium, titanium and the refractory elements. However, transient liquid-phase (TLP) bonding, which is essentially a combination of diffusion welding and brazing, has been successfully utilized in production [1]. The important step in this method is to design an interlayer alloy (filler) which does not contain any deleterious phases and has a melting point lower than that of the base metal. Boron and silicon are added to the interlayer alloys as melting-point depressants. However, the Ni – Cr – Si – B alloys which are commonly used for brazing superalloys [2], suffer from some disadvantages. Owing to the low solubility of boron in superalloy, primary block borides, which are very brittle, can form easily. Silicon has a greater solubility in the Ni_3Al phase, but it causes degeneration of high-temperature strength [3]. Even though a non-brittle joint can be produced by the TLP process, boron and silicon addition should be avoided because these elements are impurity elements in single-crystal superalloys.

Zirconium is a potential melting-point depressant in the interlayer alloys which has not as yet been evaluated. According to the Ni–Zr binary phase diagram [4], the eutectic temperature of γ (Ni) + Ni_5Zr is 1170 °C, which is about 200 °C lower than the liquidus of single-crystal superalloys. The solid solubility of zirconium in the γ′ phase was found to be 4.9 wt % (2.7 at %) in the Ni–Al–Zr system [5]. These factors make zirconium a suitable addition element for brazing materials. It is known that zirconium addition to superalloys is beneficial, because it improves the strength, ductility [6] and low-cycle fatigue life of the directionally solidified superalloys [7]. Zirconium additions are also known to counteract the harmful effects of sulphur [8] and effectively strengthen the γ′ phase [9]. The ductility of the intermetallic phase Ni_5Zr is much higher than that of the silicates and borides. By means of strain accommodation in Ni_5Zr phase at the grain boundaries, a novel series of zirconium-bearing Ni–Cr alloys referred to as boundary-phase plastic alloys (BPP alloys) has been developed [10].

The objectives of this investigation are (a) to characterize the microstructure of a zirconium-bearing interlayer alloy which is suitable for joining single-crystal superalloys, and (b) to determine the effect of zirconium on the solidification of bond layer during brazing and TLP processes.

2. Experimental procedure

The analysed compositions of the materials employed are given in Table I. DZ3 alloy was used for isothermal solidification tests in which the specimens were heated to 1370 °C, soaked for 15 min, then cooled to 1220 °C and held for 15 min of isothermal solidification at this temperature before quenching into water. The composition of zirconium-rich melts formed at interdendrites during 1220 °C isothermal solidification was analysed by energy dispersive analysis of X-rays (EDAX). The results of this analysis were used to design the zirconium-bearing interlayer alloy (alloy FZ2 in Table I) used in this investigation. Alloy

0022–2461

TABLE I Chemical composition of the alloys (wt %)

Alloy	Co	Cr	W	Mo	Al	Ti	Zr	C	B	Ni
DZ3	5.0	10.4	5.3	4.1	5.6	2.6	0.10	0.14	0.11	Base
DD3	5.2	8.9	5.3	3.1	5.6	1.6	–	0.004	–	Base
FZ2	10.4	8.5	4.4	–	–	–	13.4	–	–	Base

DD3 is a single-crystal superalloy strengthened by γ' precipitation of about 60 vol %.

The bonding tests on single-crystal superalloys were as follows: (a) a thin (about 50 μm) interlayer alloy of FZ2 was inserted between two pieces of single crystal and held together, (b) the combination specimens were sealed in quartz ampoules evacuated to 1×10^{-3} Pa and backfilled with high-purity argon to 2×10^{4} Pa pressure, and (c) the ampoules with specimens were kept at 1270 °C for 0.25, 2, 8, 24 and 48 h, respectively, furnace-cooled to below 1100 °C and then cooled in air. The microstructure of both the interlayer alloy and the bond was characterized by optical microscopy (OM), transmission electron microscopy (TEM), scanning electron microscopy (SEM), EDAX and X-ray diffraction (XRD).

Metallographic specimens were etched with a solution of 12 ml H_3PO_4, 40 ml HNO_3 and 48 ml H_2SO_4. TEM foils of the interlayer alloy were prepared by twin-jet polishing, using a solution of 64% methanol (by volume), 31% butanol and 5% perchloric acid (70% concentration) at −40 °C and 30–40 V.

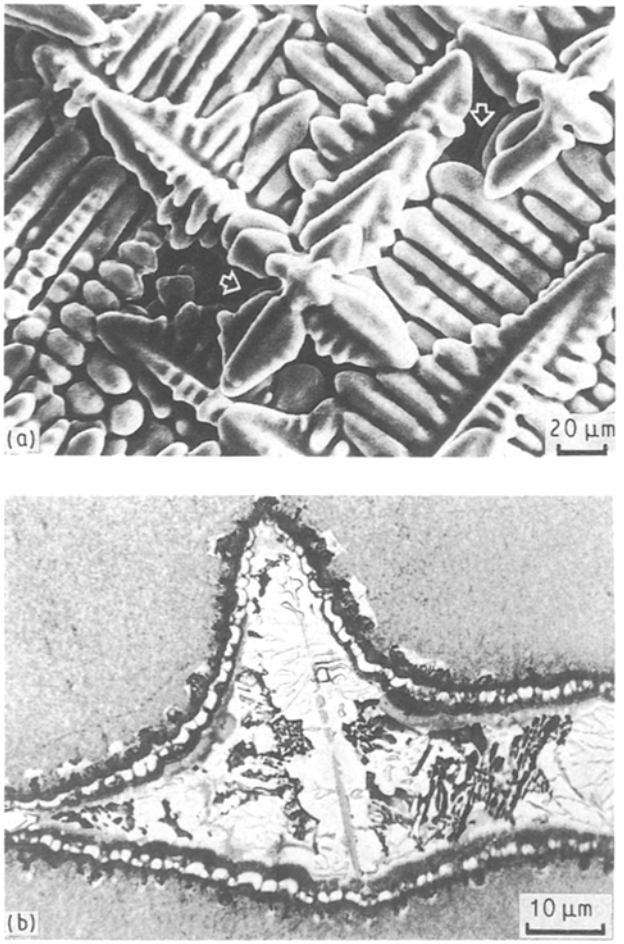

Figure 1 Microstructure of DZ 3 superalloy after isothermal solidification at 1220 °C for 15 min and water quenching: (a) morphology of the γ dendrites, the arrows indicate the pores on the surface of a specimen: (b) the low melting interdendritic region in the interior of the same specimen.

3. Results and discussion

3.1. Composition of the interlayer alloy

The morphology of γ dendrites in the DZ3 superalloy after isothermal solidification at 1220 °C for 15 min is shown in Fig. 1a. The pores on the surface of the specimen, as pointed by arrows, formed due to the flowing out of the low melting point melts from the interdendrites. In the interior of the specimen, however, interdendritic capillaries are filled with the melts, Fig. 1b. The average composition of these zones was determined by EDAX, and the results are listed in Table II.

The results indicate that zirconium is mainly distributed in the interdendrites and forms a low melting-point melt which transforms into the $\gamma + Ni_5Zr$ eutectic during cooling. This behaviour of zirconium in solidification of cast nickel-base superalloys is very similar to that of hafnium [11]. The γ dendrites formed in the early stage of solidification may be considered to be joined by the interdendritic zirconium-rich melt, therefore, the alloy composition listed in Table II may be utilized as a basic composition for the interlayer alloy. Aluminium and titanium have been left out of the interlayer alloy, because these diffuse easily into the bonds from the matrix alloys during the bonding cycle. However, tungsten, which is an important strengthening element for both the γ and the γ' phases, diffuses very slowly and as such must be incorporated into the interlayer alloy. Molybdenum, another strengthening element and a slow diffuser, is, however, excluded as its role can be provided by adjusting the amount of tungsten in the interlayer alloy. The final composition which is based on the above considerations is as follows: Ni–10Co–8Cr–4W–13Zr.

3.2 Microstructure of the interlayer alloy

The microstructure of the as-cast FZ2 alloy is hypoeutectic and consists of the primary γ and $\gamma + Ni_5Zr$ eutectic, as shown in Fig. 2. A closer examination of the eutectic at a higher magnification, as seen in Fig. 3, shows that this eutectic consists of γ bars surrounded by the phase Ni_5Zr instead of the apparent lamellar and cellular structures.

The existence of the Ni_5Zr phase in the as-cast FZ 2 alloy was confirmed by X-ray diffraction of

TABLE II Composition of interdendritic zone of DZ3 alloy after the isothermal solidification at 1220 °C for 15 min (wt %)[a]

Ni	Co	Cr	W	Mo	Al	Ti	Zr
55.46	5.01	12.09	1.52	8.84	2.24	3.01	12.09

[a] Carbon and boron were not determined.

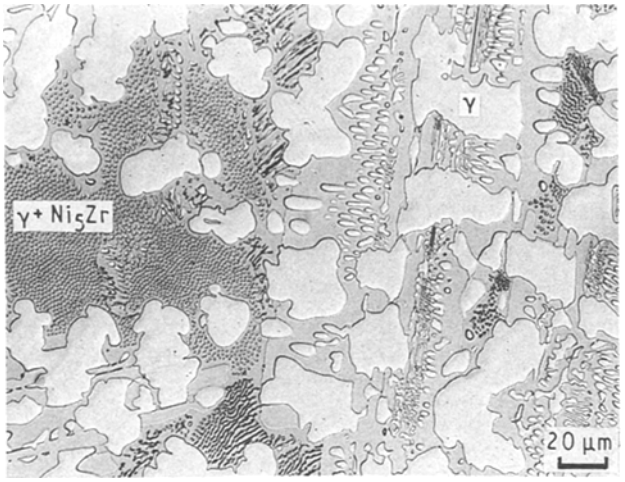

Figure 2 Microstructure of the as-cast interlayer alloy FZ2, showing the primary γ dendrites and γ + Ni_5Zr eutectic.

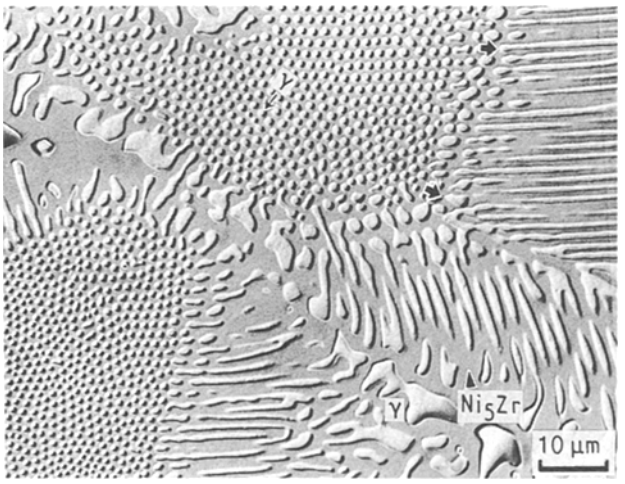

Figure 3 Morphology of the γ + Ni_5Zr eutectic showing different orientation of the γ bars in neighbouring colonies.

powder specimens, as shown in Fig. 4. A TEM study was also undertaken on the as-cast FZ 2 alloy, and the Ni_5Zr phase with f c c structure was identified. Fig. 5a shows the γ phase in a matrix of Ni_5Zr phase. Fig. 5b is a diffraction pattern showing a $[0\ 1\ 3]_{Ni_5Zr}$ zone axis and Fig. 5c shows $[1\ 1\ 2]_{Ni_5Zr}$ zone axis and $[0\ \bar{1}\ \bar{1}]_\gamma$ zone axis which give the orientation relationship between γ and Ni_5Zr: $\{1\ 1\ \bar{1}\}_{Ni_5Zr}//\{\bar{1}\ 1\ \bar{1}\}_\gamma$ and $\langle 1\ 1\ 2\rangle_{Ni_5Zr}//\langle 0\ \bar{1}\ \bar{1}\rangle_\gamma$.

The composition of various phases in the FZ 2 alloy was determined by EDAX. The results are listed in Table III. It is seen that except for the higher solubility of cobalt, other elements have very low solubility in the Ni_5Zr phase. It has been reported that the solubility of zirconium in Ni_5Zr is 22.2 wt % in the binary Ni–Zr alloys containing 1.24–14.43 wt % Zr [5], which is close to our observed value of 24.3 wt %. These values are also in agreement with the value of 21.5–26 wt % Zr reported in the binary phase diagram of Ni–Zr [4]. Thus, it is seen that the zirconium content in Ni_5Zr is rather constant for both the binary and the interlayer multicomponent Ni–Zr alloys. This suggests that elements such as cobalt and chromium are substituted mainly for nickel atoms in the Ni_5Zr phase. The composition of Ni_5Zr in the alloy studied is here quite similar to that of Ni_5Zr observed in zirconium bearing nickel-base superalloy [7].

Table III shows that the room-temperature solubility of zirconium in primary and eutectic γ phase is 0.6 and 0.4 wt %, respectively. This is much smaller than the value of 1.2 wt % reported by Huffstutler and Petersen [12], but close to the value of 0.2 at % obtained by Kirkpatrick and Larsen [13]. Whereas the solubility of zirconium in the γ phase is very low, cobalt, chromium and tungsten show a considerable solubility. Tungsten is a negative segregation element in the FZ 2 alloy; therefore, its content in the primary γ is much higher than that in the eutectic γ.

Microhardness measurements at 50 g loads on Ni_5Zr phase in the interlayer FZ 2 alloy gave an average value of 4541 MPa which is much higher than the value of 981–1079 MPa obtained by Huffstutler in the binary Ni–Zr alloys [12]. It is suggested that this increased hardness is due to solid-solution strengthening by cobalt, chromium and tungsten. Despite this higher hardness of the Ni_5Zr phase, the FZ 2 alloy was rather ductile and was not fragmented during hammering.

3.3. Bonding behaviour of interlayer alloy

The liquidus and solidus temperatures of the single-crystal superalloy are 1380 and 1310 °C, respectively, whereas the liquidus temperature of the interlayer alloy is 1220 °C. There is a 90 °C temperature gap between the solidus of the base alloy and the liquidus of the interlayer alloy, which provided some degree of freedom in the choice of the bonding temperature. Preliminary tests showed that the melted interlayer alloy had the necessary fluidity and wettability at 1270 °C to fill the gap between the base alloy. The bond in Fig. 6 was produced in 15 min at 1270 °C. The light zone is the γ solid solution. The γ + Ni_5Zr eutectic exists in the centre of this band. The average thickness of this band is 140 μm which is larger than the original gap of about 60 μm width. Chemical reaction of the liquid and the adjacent base metal increases

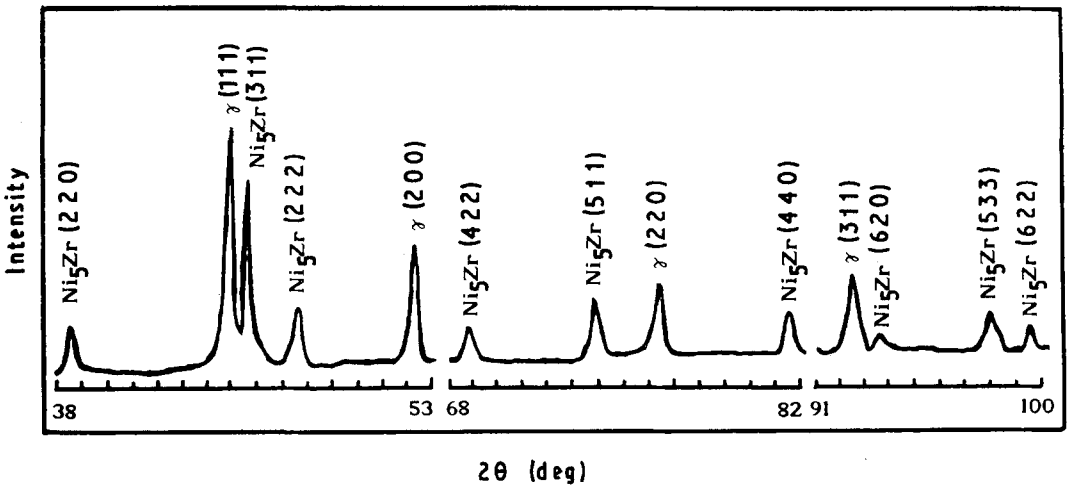

Figure 4 X-ray diffraction of as-cast FZ2 alloy, CuK_α radiation.

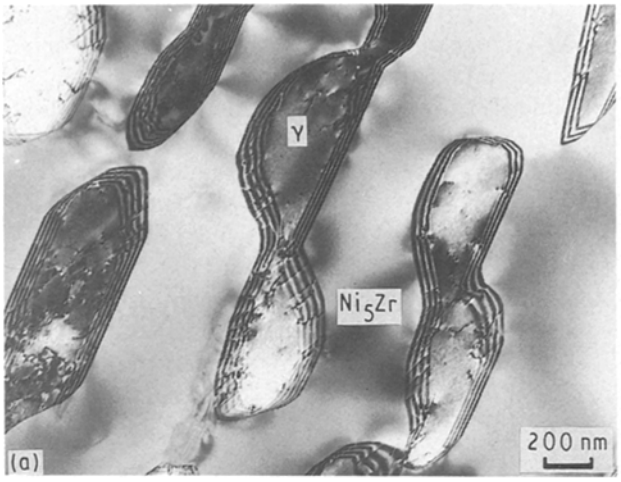

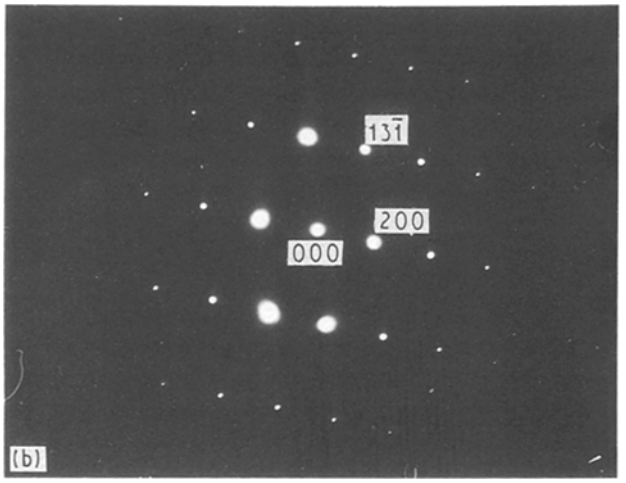

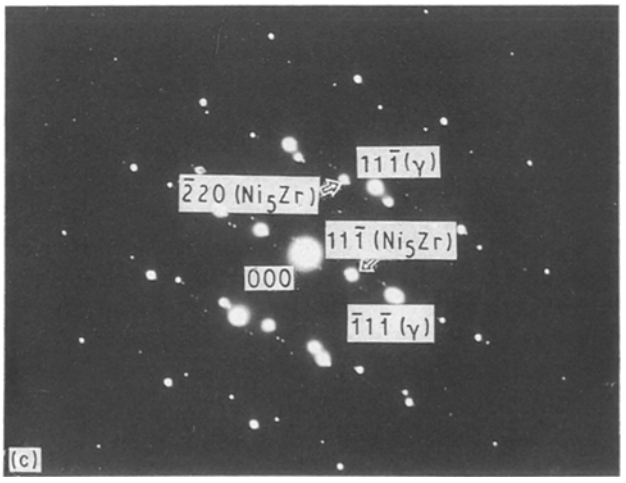

Figure 5 Transmission electron micrograph and diffraction patterns of the $\gamma + Ni_5Zr$ eutectic: (a) TEM view of the $\gamma + Ni_5Zr$ eutectic region, (b) diffraction pattern of the Ni_5Zr phase, showing the zone axis [0 1 3], and (c) diffraction pattern from the $\gamma + Ni_5Zr$ region showing zone axis $Z = [1\ 1\ 2]_{Ni_5Zr}//[0\ \bar{1}\ \bar{1}]_\gamma$.

the zirconium content at the base metal surface causing it to melt. The local melt-back of the mating surfaces decreases the concentration of zirconium in the liquid interlayer and enlarges the melted zone. Thus, the width of the melt zone after 15 min at 1270 °C is approximately 140 μm. The microsegregation in both the base metal and the bond is not removed due to the absence of sufficient time for diffusion. This is a typical brazing microstructure.

The microstructure of the bond after 2 h at 1270 °C and subsequent furnace cooling is presented in Fig. 7 where the melt zone (MZ), the isothermal solidification zone (ISZ) and the eutectic zone (EZ), formed during furnace cooling are marked. The average width of the melt zone is similar to that found in the sample heated for only 15 min. This indicates that after about 15 min heating at 1270 °C, further melting of the base-metal surface ceases and the isothermal solidification process begins because of the continuing diffusion of zirconium and cobalt away from the joint and enrichment of the melt with base-metal elements. From metallographic examination of specimens quenched from various temperatures, it was determined that the $L \rightarrow \gamma + \gamma'$ eutectic reaction occurs at 1220 °C and the $L \rightarrow \gamma + Ni_5Zr$ eutectic reaction takes place at 1150 °C. These results are in agreement with DTA results for the zirconium-bearing nickel-base superalloys [14]. Thus during cooling, a portion of the liquid left at the end of the isothermal solidification process transforms to the flower-shaped eutectic

TABLE III Composition of phase in the interlayer alloy (wt %)

Phase	Ni	Co	Cr	Zr	W
Primary γ	59.77	14.43	14.80	0.57	10.47
Eutectic γ	65.40	15.25	14.40	0.40	4.55
Eutectic Ni_5Zr	67.97	5.53	1.57	24.37	0.70

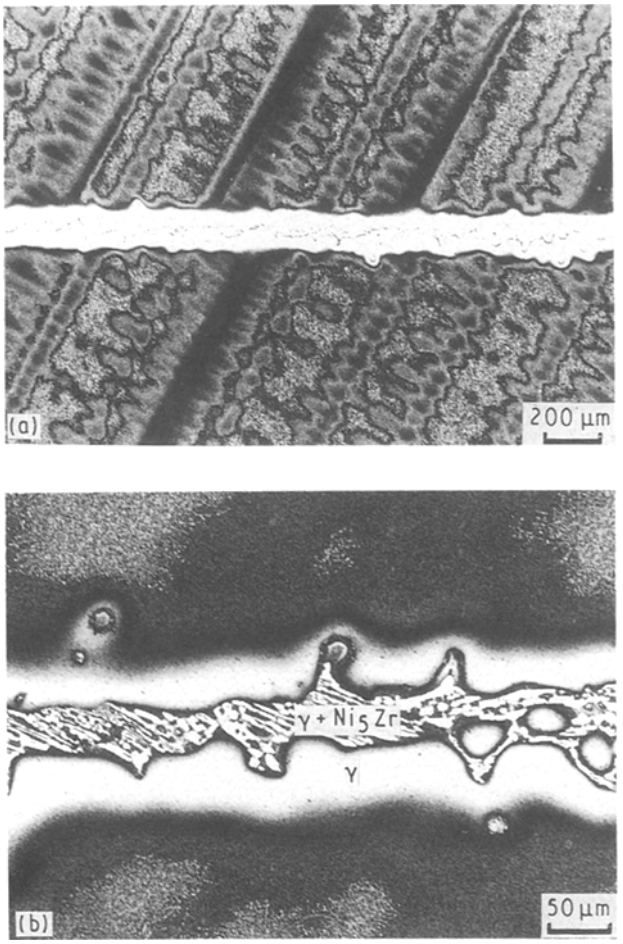

Figure 6 Microstructure of the bond made at 1270 °C for 15 min in DD3 single-crystal superalloy: (a) dendrites in the base alloy and γ solid solution in the bond (light zone), (b) the γ phase and the $\gamma + Ni_5Zr$ eutectic.

$\gamma + \gamma'$ at 1220 °C and the balance to a cellular eutectic of $\gamma + Ni_5Zr$ at 1150 °C. On further cooling, γ' is precipitated out in the γ phase of the cellular eutectic. It may be noted that this again is a typical brazing structure.

The average composition across the bond into the base metal was determined by EDAX and the results are listed in Table IV. It may be seen that the diffusion distance of zirconium in the base alloy is rather large (about 230 μm) after isothermal solidification at 1270 °C for 2 h and subsequent cooling. Further analytic work on individual phases, however, showed that the solubility of zirconium in the γ and γ' phases is very different, namely, 0.29 and 1.29 wt %, respectively. The elements aluminium and titanium are seen to be easily replenished at the bond by diffusion from the base metal. The concentrations of aluminium and titanium near the bond are close to that in the base

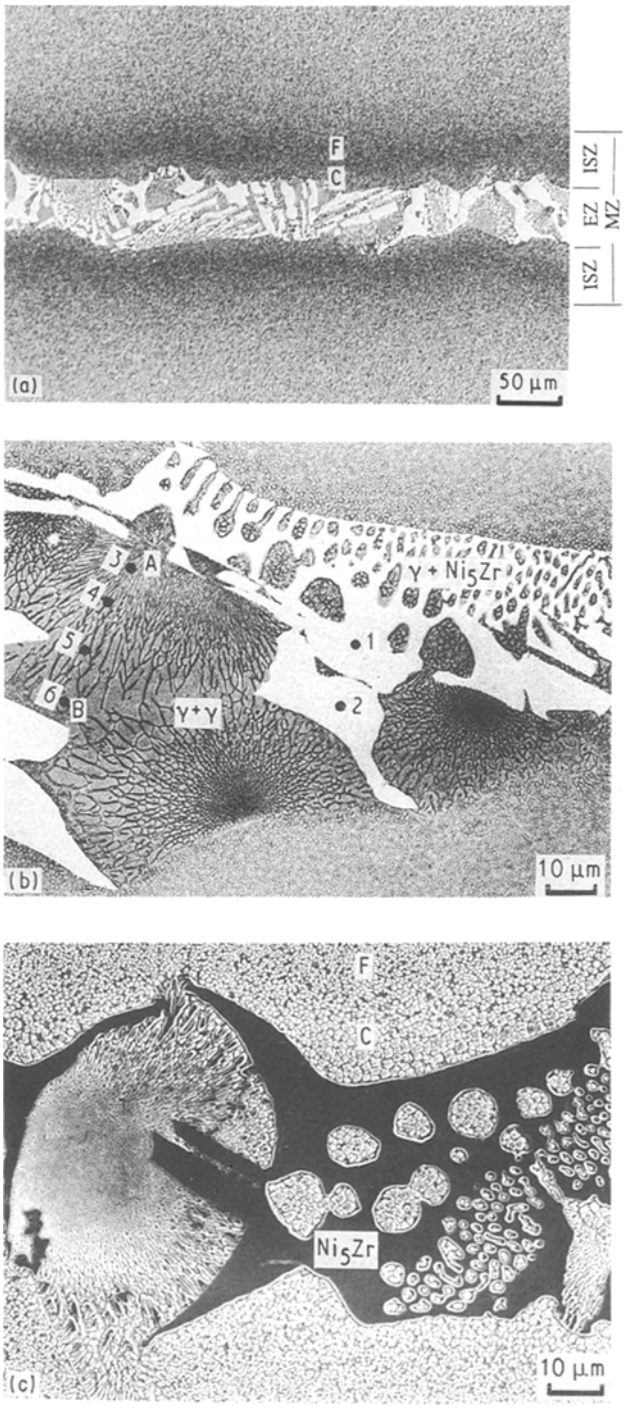

Figure 7 Microstructure of the bond after 1270 °C for 2 h: (a) the melt zone (MZ), the isothermal solidification zone (ISZ) and the eutectic zone (EZ); (b) the $\gamma + \gamma'$ eutectic and $\gamma + Ni_5Zr$ eutectic formed in the EZ zone, 1–6 indicate the points where the analyses were performed and the results are given in Table V; (c) fine γ' zone (F) and coarse γ' zone (C) in the ISZ zone.

alloy. During cooling below 1200 °C, secondary γ' phase precipitates in the isothermally solidified zone where the concentration of γ' formers such as aluminium, titanium and zirconium is sufficiently high;

TABLE IV The average composition across the bond into the base metal

	Determined point					
	1	2	3	4	5	6
Distance from the end of eutectic zone (μm)	0	50	100	150	200	250
Ni (wt %)	71.81	72.06	74.91	72.83	74.78	74.89
Cr (wt %)	8.20	9.65	5.01	8.84	6.50	6.90
Zr (wt %)	0.77	0.30	0.23	0.20	0.14	0.00
Ti (wt %)	1.21	0.97	1.88	1.44	1.78	1.70
Al (wt %)	4.76	3.40	6.75	4.71	5.84	5.73
Mo (wt %)	1.43	2.38	2.09	2.59	2.31	2.16
W (wt %)	4.82	4.53	5.39	4.49	4.51	4.33
Co (wt %)	7.09	6.71	3.75	4.92	4.15	4.28

TABLE V Analysis of different areas in the eutectic zone (Fig. 7b)

Element	Composition (wt %)					
	1	2	3	4	5	6
Ni	70.84	69.42	76.48	76.77	76.63	77.03
Cr	0.70	0.94	5.08	4.53	3.59	3.42
Zr	22.41	23.26	1.66	1.94	2.72	2.94
Ti	0.28	0.24	2.00	2.16	2.25	2.19
Al	0.47	0.56	6.51	6.58	6.99	7.16
Mo	0.00	0.18	1.08	1.04	1.03	0.80
W	0.74	0.64	2.22	2.00	2.12	1.57
Co	4.55	4.95	4.97	4.98	4.67	4.89

therefore, there is no γ'-depleted zone in the vicinity of the eutectic zone.

Quantitative analysis of different areas in the eutectic zone in Fig. 7a was performed, and the results are given in Table V. Points 1 and 2 in Fig. 7b represent the Ni_5Zr phase, and points 3, 4, 5 and 6 are all distributed within the flower-shaped colony of $\gamma + \gamma'$ eutectic. Among them, 3 and 4 represent $\gamma + \gamma'$ and points 5 and 6 are single-phase γ'. It is noted that the concentrations of zirconium and aluminium progressively increased from point 3 to point 6, and correspondingly the volume per cent of γ' from the start of eutectic (A region) to the edge of eutectic $\gamma + \gamma'$ (B region) increases due to increasing amounts of γ'-formers aluminium and zirconium.

To achieve high strength in the bond it is necessary to have higher amounts of γ' and no low melting phase in the bond region. Our results show that the elements aluminium and zirconium play an important role in determining the quantity, size and morphology of the γ' phase. In the isothermal solidification zone, the size and shape of the γ' phase are very different and depend upon their location: the coarse cubic-shaped γ' exists in a 20 μm wide band starting from the edge of the eutectic zone (region C), and next to this band lies another band of 30 μm width containing fine spherical γ' (region F). Referring to Table IV and Fig. 7a and 7c, it is seen that points 1 and 2 in Table IV correspond to areas C and F, respectively, in Fig. 7a and c. The higher total content of aluminium, titanium and zirconium at point 1 is considered to be the reason for the formation of coarse γ'.

Zirconium promotes the formation of both the secondary γ' and the eutectic γ' [7]. The data listed in Table V show that the maximum solid solubility of zirconium in the eutectic γ' is 2.9 wt % (1.8 at %), lower than the values of 2.0 [9] and 2.7 at % [5] reported earlier in work on the Ni–Al–Zr ternary system. Because zirconium has a large solubility in the eutectic γ' and the volume per cent of γ' in eutectic $\gamma + \gamma'$ is much higher than that of γ, the eutectic reaction $L \rightarrow \gamma + \gamma'$ consumes large amounts of zirconium; as a result, the eutectic reaction $L \rightarrow \gamma + Ni_5Zr$ is suppressed and the compound Ni_5Zr in the bond is replaced by eutectic γ'.

Zirconium is an effective γ'-strengthener. It has been reported that the microhardness of Ni_3 (Al, Zr) containing 3 at % Zr is 2157 MPa higher than that of Ni_3Al (3040 and 5198 MPa for Ni_3Al and Ni_3(Al, Zr), respectively) [9]. From the above, it is seen that zirconium can decrease the melting point of the interlayer alloy for brazing and at the same time facilitate the precipitation of γ' to provide strength in the bond.

As the holding time at temperature is increased, the concentration of zirconium in the eutectic zone decreases, as a consequence, there is a corresponding decrease in the amount of Ni_5Zr in the bond. The result of isothermal solidification for 8 h at 1270 °C is shown in Fig. 8. It is noted that the Ni_5Zr phase has become more discontinuous and its quantity is de-

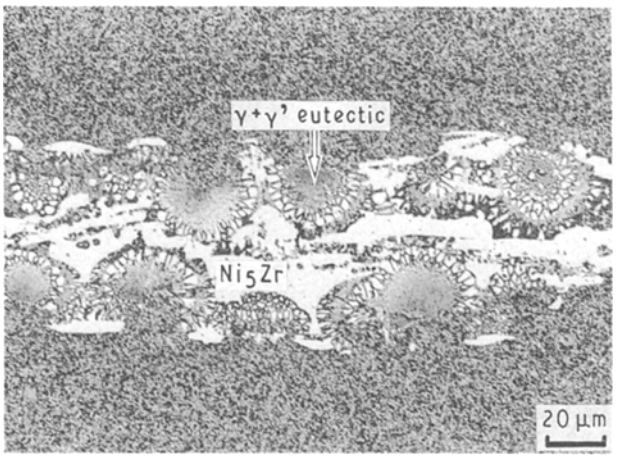

Figure 8 Microstructure of the bond after 1270 °C for 8 h.

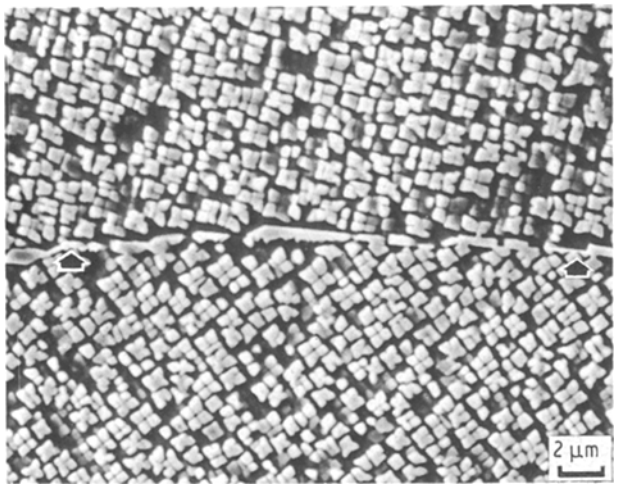

Figure 9 Typical TLP microstructure of the bond after 1270 °C for 48 h. Secondary γ′ is uniformly distributed in the γ phase. The arrows indicate the grain boundary formed by the two pieces of single crystal with different orientation.

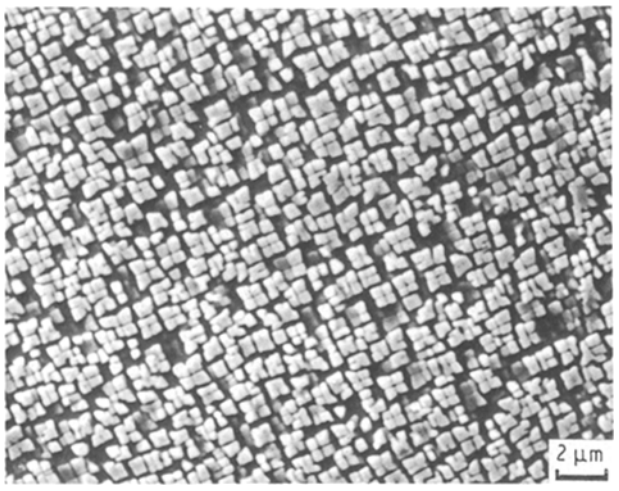

Figure 10 Morphology of the secondary γ′ phase in the base alloy.

creased, i.e. part of it is replaced by the eutectic γ + γ′. This trend continues with increasing time for isothermal solidification, until after 48 h no Ni_5Zr or eutectic γ′ is left and the secondary γ′ is uniformly distributed in a matrix of γ (Fig. 9) which is the microstructure of the base alloy (Fig. 10). Thus it is clear that TLP bonding of single-crystal superalloy, without the use of silicon and boron can be achieved by incorporating zirconium in the interlayer alloy.

4. Conclusions

1. The concentration of zirconium in the residual liquid at the interdendrites can reach 10 wt % during later stages of solidification. Guided by this information, an interlayer alloy containing Ni–10 Co–8 Cr–4 W–13 Zr was selected for bonding single-crystal nickel-base superalloy. The solubility of zirconium in the γ phase is 0.6 wt % and the content of zirconium in the Ni_5Zr phase is rather constant (about 24 wt %). In the γ + Ni_5Zr eutectic, the two phases have an orientation relationship of $\{1\ 1\ \bar{1}\}_{Ni_5Zr} // \{\bar{1}\ 1\ \bar{1}\}_\gamma$ and $\langle 1\ 1\ 2\rangle_{Ni_5Zr}Zr // \langle 0\ \bar{1}\ \bar{1}\rangle_\gamma$.

2. Using the above alloy, bonds free of brittle phases in the single-crystal superalloy have been obtained by isothermal solidification at 1270 °C for 48 h.

Acknowledgements

This research was supported by the Natural Sciences and Engineering Council Canada and the Office of Research Administration, the University of Manitoba. The technical assistance from D. Mardis and J. Van Dorp is gratefully acknowledged. Thanks are also due to the Beijing Institute of Aeronautical Materials for supplying the alloys.

References

1. D. S. DUVALL, W. A. OWCZARSKI and D. F. PAULONIS, *Welding J.* **53** (4) (1974) 203.
2. E. F. BRADLEY, in "Superalloys – a Technical Guide" (ASM International, Metals Park, OH, 1988) p. 222.
3. V. V. SIDOROV, G. I. MOROZOV, N. V. PETRUSHIN, E. A. KULEBYAKINA and L. I. DMITIEVA, *Russ. Metall.* **1** (1990) 92.
4. T. B. MASSALSKI, J. L. MURRAY, L. H. BENNETT and H. BAKER, in "Binary Alloy Phase Diagram", Vol. II (ASM, Metals Park, OH, 1986) p. 1779.
5. E. R. THOMPSON and F. D. LEMKEY, *Trans. ASM* **62** (1969) 140.
6. D. N. DUHL, US Pat. 3700 433 (1972).
7. Y. ZHENG, Y. WANG, J. XIE, P. CARON and T. KHAN, in "Proceedings of the 6th International Conference on Superalloys", Pennsylvania, September 1988, edited by S. Reichman, D. N. Duhl, G. Maurer, S. Antolovich and C. Lund (The Metallurgical Society, 1988) p. 335.
8. J. E. DOHERTY, A. F. GIAMEI and B. H. KEAR, *Canad. Metall. Q.* **13** (1) (1974) 229.
9. J. E. DOHERTY, B. H. KEAR and A. F. GIAMEI, *J. Metals* **23** (11) (1971) 59.
10. P. J. PARRY, P. J. BRIDGES and B. TALOR, *J. Inst. Metals* **97** (1969) 373.
11. Y. ZHENG and C. LI, in "Proceedings of the 6th International Conference on Superalloys", Pennsylvania, September 1988, edited by S. Reichman, D. N. Duhl, G. Maurer, S. Antolovich and C. Lund (The Metallurgical Society, 1988) p. 475.
12. M. C. HUFFSTUTLER Jr. and O. G. PETERSEN, *J. Inst. Metals* **95** (1967) 23.
13. M. E. KIRKPATRICK and W. L. LARSEN, *Trans. ASM* **54** (1954) 580.
14. S. MA, Y. ZHENG and Y. CAI, *Acta Metall. Sinica* **17** (1981) 522.

Received 3 January
and accepted 25 June 1992